Nanostructured Organic–Inorganic Copolymer Networks Based on Polymethacrylate-Functionalized Octaphenylsilsesquioxane and Methyl Methacrylate: Synthesis and Characterization

ARTICLE *in* MACROMOLECULES · JANUARY 2011

Impact Factor: 5.8 · DOI: 10.1021/ma102047m

566 *Macromolecules* **2011**, *44*, 566–574
DOI: 10.1021/ma102047m

Macromolecules
ARTICLE

Nanostructured Organic−Inorganic Copolymer Networks Based on Polymethacrylate-Functionalized Octaphenylsilsesquioxane and Methyl Methacrylate: Synthesis and Characterization

Zhanbin Wang, Shiwei Leng, Zhonggang Wang,* Guiyang Li, and Hao Yu

Department of Polymer Science and Materials, State Key Laboratory of Fine Chemicals, School of Chemical Engineering, Dalian University of Technology, Dalian 116012, People's Republic of China

Received June 21, 2010; Revised Manuscript Received December 13, 2010

ABSTRACT: Novel polymethacrylate-functionalized octaphenylsilsesquioxanes (OPS) macromonomer was designed and synthesized, which was employed as nanofiller and cross-linker to copolymerize with MMA to produce OPS/PMMA hybrid nanocomposites with OPS contents ranging from 0 to 1.18 mol %. The synthesis route was that, OPS was brominated to yield polybromo-OPS, and polybromo-OPS was then reacted with BuLi and CO_2 to obtain polycarboxyl-OPS. After that, the carboxyls were converted to chlorocarbonyl groups, and the esterification reaction of polychlorocarbonyl-OPS with 2-hydroxyethyl methacrylate led to polymethacrylate-OPS. Their chemical structures were characterized by means of FTIR, ^{1}H NMR and ^{13}C NMR spectra. Moreover, after cleavage of C−Si bond by KF/H_2O_2, the position and number of functional groups on the benzene rings of OPS macromonomers and the molecular weight of PMMA in the nanocomposite were investigated in detail by LC−MS and GPC methods, respectively. The prepared OPS macromonomer can result into PMMA significantly improved thermal-chemical stability and apparently increased glass transition temperature. For example, the nanocomposites are insoluble in any common organic solvents due to the formation of three-dimensional networks. Compared to the pure PMMA, the OPS/PMMA nanocomposite with OPS content of only 0.94 mol % exhibits increased 5%-mass-loss temperature and glass transition temperature by 104 and 21 °C, respectively.

Introduction

Polyhedral oligomeric silsesquioxanes (POSS), in both nanoscience and nanomaterials, continue to receive considerable attention owing to their unique molecular characteristics such as the robust inorganic silica core surrounded by the identical or different organic groups, precisely controlled monodispersed nanometer size (ca. 1−2.5 nm in diameter), and diverse synthetic strategies for organic functionalization.[1−7] Of particular interest are chemically bonded POSS/polymer hybrid nanocomposites, wherein even very small amount of POSS particles uniformly distributed within the polymer matrix at the nanometer scale bring about significant improvement in heat-resistance, dimensional stability and mechanical properties of the materials.[8−17]

One of the most important aspects in POSS-chemistry is its functionalization with the aim to produce POSS macromonomers that can be used in linear, branching or cross-linking copolymerization reactions with other monomers. Depending on the number of pendant reactive groups, POSS can be classified as monofunctional,[18,19] bifunctional[20] and polyfunctional[21,22] compounds. Monofunctional cubic POSS are usually achieved through vertex-capping of incompletely condensed POSS trisilanols with $RSiCl_3$ (R is a functional group) and which, including vinyl-POSS, acrylate-POSS, methacrylate-POSS, and styryl-POSS,[18,19,23−25] have been copolymerized with methyl methacrylate (MMA) or styrene via free radical polymerization to obtain linear poly(methyl methacrylate), polystyrene or their copolymers bearing pendant POSS side groups, whereas epoxy-POSS, amino-POSS, and carboxyl-POSS are covalently incorporated into cured epoxy networks or used for the preparations of POSS/polyamide nanocomposites.[26−29] In addition, Leu et al synthesizes a bifunctional diamino-POSS macromonomer through the vertex-capping reaction, which together with 4,4′-oxidianiline, is polymerized with pyromellitic dianhydride to afford linear POSS/polyimide hybrid materials.[30]

Relative to mono- or bifunctional POSS, polyfunctional POSS are preferred since the formed branched, star-shape and cross-linked hybrid structures can more tightly tethered the polymer with POSS through multiple covalent conjunctions, and thereby significantly improve its physical properties compared to the linear one. In earlier work, polyfunctional POSS are often obtained through hydrosilylation of unsaturated compounds with $(HSiO_{1.5})_8$ or $(HMe_2SiO_{1.5})_8$ such as octavinyl-POSS,[21] octamethacryalte-POSS,[22,30] and octahydroxy-POSS.[31] However, the synthesis route utilizing hydrosilylation often gives rise to functional groups linked with POSS cores through aliphatic segments, which results into nanocomposite the low thermal and mechanical stability compared to the aromatic analogues, and consequently limits their application field to some extent.

Over the past decade, the study of completely condensed aromatic octaphenylsilsesquioxane (OPS) has become an active research area owing to its high thermal stability. Moreover, the presence of eight phenyls provides an opportunity for functionalization. However, a review of literature reveals that, up to now, only few types of polyfunctional OPS are reported except for the polybromo-OPS and octanitro- and octaamino-OPS (OAPS) synthesized by Laine et al.[32,33] OAPS has been employed as a building block to synthesize rigid cross-linked polyimides, as macromolecular curing agents to prepare thermosetting epoxy

*To whom all correspondence should be addressed. E-mail: zgwang@dlut.edu.cn.

 Published on Web 01/05/2011

resins, or converted to octafunctionalized maleimide resins.[34−36] Thereafter, Zheng et al uses OAPS to prepare photocurable octacinnamamidophenyl silsesquioxane, which is then photo-cross-linked with polyvinylcinnamate (PVCIN) to yield the OPS/PVCIN nanocomposites.[37]

To further exploit the potential of OPS and extend the type of functionalized OPS macromonomers, herein we design and synthesize polycarboxyl-OPS and polychlorocarbonyl-OPS, which offer an access to a variety of novel polymer/inorganic nanocomposites. For example, polychlorocarbonyl-OPS can be applied for the preparations of hyperbranched or cross-linked polyesters or polyamides, whereas polycarboxyl-OPS may provide a possibility to construct micro/mesoporous rigid polybenzoxazoles, or as macromolecular curing agents to synthesize thermosetting epoxy resins. Besides, through the reaction of polychlorocarbonyl-OPS with 2-hydroxyethylmethacrylate, polymethacrylate-OPS has been readily obtained.

Poly(methyl methacrylate) is a transparent amorphous thermoplastic engineering material widely used in wide range of industrial fields. However, its chemical resistance and thermal stability have to be improved to meet the increasing demands of property for advanced electronic and optical applications. Cross-linking can be an effective way to enhance chemical and thermal stability by using diol dimethacrylate, divinylbenzene, aromatic phenolphthalein dimethacrylate, poly(2-acryloyloxyethyl methacrylate), and poly(2-methacryloyloxyethyl methacrylate) as cross-linking agents.[38−41] Recently, polyvinyl-POSS derived from hydrosilylation reaction is copolymerized with MMA, and thus formed POSS/PMMA networks show enhanced thermal/mechanical properties.[30,42,43]

The aim of the present work is to synthesize new polymethacrylate-OPS macromonomers, and then the mixtures of polymethacrylate-OPS and MMA with OPS contents from 0 to 1.18 mol % are copolymerized to produce OPS/PMMA nanocomposites with an expectation to significantly improve the chemical resistance and thermal property of PMMA material.

Experimental Section

Materials. Phenyltrichlorosilane was purchased from J&K-Chemical Co., Ltd. Octaphenylsilsesquioxane (OPS) was synthesized via hydrolysis and condensation of phenyltrichlorosilane according to the procedure in the literature[44] with 87% yield. 2-Hydroxyethylmethacrylate (HEMA) and MMA were purchased from Tianjin Chemical Reagent Co., and distilled under reduced pressure from hydroquinone and calcium hydride prior to use. Azobis(isobutyronitrile) (AIBN) was purchased from Shanghai Reagent. Benzene and THF were refluxed over sodium and distilled just before use. Pyridine was purified by distillation under reduced pressure from calcium hydride. The other solvents were of reagent grade and used as received.

Instrumentation. Fourier transform infrared (FTIR) spectra were recorded on a Nicolet-20DXB IR spectrometer at room temperature in the 400−4000 cm^{-1} region with a resolution of 2 cm^{-1}. Liquid samples were measured by casting film on KBr salt tablets, whereas solid samples were prepared by dispersing the sample in KBr and compressing the mixtures to tablets.

^1H NMR and ^{13}C NMR were carried out on a Varian INOVA400 spectrometer at room temperature. The NOE-suppressed ^{13}C NMR spectra were accumulated with the slowly changing homogeneity of the magnetic field. Typically pulse delay of 10 s, acquisition times of 0.5 s, and a 2500 Hz sweep width were utilized.

Gel permeation chromatography (GPC) analysis was conducted with a PL-GPC220 system using PS as standard and tetrahydrofuran (THF) as the eluent.

Elemental analyses were determined with an Elementar Vario EL III elemental analyzer.

High performance liquid chromatography (LC) analysis was conducted on HP1100LC/MSD instrument with a Zorbax Extend C18 (2.1 × 150 mm) column with mobile phase of mixed solution containing 89.9% of methanol, 10% of water and 0.1% of formic acid. Detection was at 254 nm, and a flow rate was constant at 0.2 mL/min. Mass selective detector (MS) analysis was conducted with an HP1100 Series MSD system.

Differential scanning calorimetry (DSC) was run on NETZSCH DSC204 at the temperature of 100−350 °C at a heating rate of 10 °C/min in nitrogen atmosphere. The glass transition temperatures (T_g) were read at the middle of the change in the heat capacity.

Wide angle X-ray diffraction (WAXD) study of the powder sample was performed using Rigku D/max-2400 X-ray diffractometer (40 kV, 200 mA) with a copper target at a scanning rate of 2°/min, scanned from 5 to 60°.

Thermal gravimetric analysis (TGA) was carried out on the NETZSCH TG209C under nitrogen atmosphere in the 50−600 °C region with a heating rate of 20 °C/min.

Synthesis of Polybromo-OPS. Polybromooctaphenylsilsesquioxane (polybromo-OPS) was prepared in reference to the procedure reported in the literature with some modifications:[32] 30 g of OPS (0.232 mol-phenyl), 2.85 g (0.051 mol) of iron powder, and 200 mL of dichloromethane were added into a 500 mL round-bottom flask equipped with magnetic stirring. Then, 13.4 mL of Br_2 (0.261 mol) was added dropwise over a period of 30 min at room temperature under the atmosphere of nitrogen. The mixture was stirred for 6 h. Then 50 mL of 10% aqueous $NaHSO_3$ was added to terminate the reaction. The organic layer was separated and washed with deionized water three times, and the solvent was removed by rotary evaporation. The crude product was dissolved in 60 mL of ethyl acetate and precipitated into 200 mL of methanol. The solution was filtered to afford 43 g white solid with the yield of 85%. Anal. Found: C, 34.42; H, 1.94; Br, 39.57. FTIR (cm^{-1}): 3069, 1578, 1102, 1067, 1010. ^1H NMR (DMSO-d_6, ppm): 6.9−8.0 ppm. ^{13}C NMR (DMSO-d_6, ppm): 6.9−8.0 ppm; 135.8, 133.4, 132.2, 131, 128.1, 126.2, 122.1, 120.6. GPC: M_n = 1457, M_w = 1493, M_w/M_n = 1.02.

Synthesis of Polycarboxyl-OPS. A dry four-neck flask, fitted with thermometer, nitrogen, and carbon dioxide inlet tubes and dropping funnel, was charged with 80 mL of anhydrous tetrahydrofuran and 12 g of polybromo-OPS. While maintaining the temperature at −78 °C, 60 mL of BuLi (2.5 M in hexane) was charged dropwise over a period of 2.5 h under the protection of nitrogen. It was observed that a white precipitate appeared because of the formed lithium compound. Then the CO_2, dried through a molecular sieve column, was flowed into reaction flask for another 14 h. The reaction was terminated by adding 10 mL methanol, 20 mL water and finally 5 mL 2N dilute aqueous HCl. The precipitate was filtered and dried to afford 7.6 g white powder with 77% yield. Anal. Found: C, 44.82; H, 2.97; Br, 2.71. FT-IR (cm^{-1}): 2800−3700, 3064, 1697, 1596, 1167; ^1H NMR (D_2O/NaOH, ppm): 6.9−8.0 (m, Ar−H). ^{13}C NMR (D_2O/NaOH, ppm): 182.6, 176.3, 172.1, 146.8, 142.9, 140.1, 137.1, 134.9, 134.1, 133.9, 132.1, 130.6, 131.1, 128.3, 126.8, 122.1, 120.5.

Synthesis of Polychlorocarbonyl-OPS. A 500 mL four-necked flask was equipped with a mechanical stirrer, nitrogen inlet and outlet and a condenser, using a bubbler trap containing aqueous NaOH attached to the end of condenser to absorb the released SO_2 gas. After 6 g of polycarboxyl-OPS, 250 mL of newly distilled thionyl chloride ($SOCl_2$) and 1.5 mL of pyridine were added, the system was heated gradually to refluxing temperature. It was observed that, with the reaction time, the polycarboxyl-OPS solid began to dissolve, and disappeared completely to become a homogeneous solution. Then the reaction was allowed to proceed at this temperature for 12 h. The excess $SOCl_2$ was distilled out under reduced pressure. The residual trace $SOCl_2$ was further removed by azeotropic distillation with

benzene three times. Thus 5.3 g of white solid was obtained in 73% yield, which was directly used for the preparation of polymethacylate-OPS.

Synthesis of Polymethacylate-OPS. At room temperature, to a 500-mL three-necked flask equipped with a mechanical stirrer, dry nitrogen inlet and outlet, a condenser, and a dropper was charged 150 mL of benzene, 5.3 g of polychlorocarbonyl-OPS, and 3.5 mL of pyridine. Then a solution of 2-hydroxyethylmethacrylate (HEMA) (34.2 g, 58.59 mmol in 30 mL of dried benzene) was added dropwise under stirring to the above mixture over a 1 h period. After reacting overnight, 0.1 g of hydroquinone was added and the solvent was distilled out under reduced pressure to give a pale yellow solid. The crude product was dissolved in ethanol and precipitated into the water. Repeating the above purification procedure three times gave 5.5 g of a white solid. Yield: 82%. FTIR (cm^{-1}): 3075, 2960, 2934, 1724, 1134, 1011. ^1H NMR (DMSO-d_6, ppm): 5.61−6.05 (=CH−), 3.62 and 4.09 ($-CH_2-O$), 1.88 ($-CH_3$), 7.32−7.91 (Ar−H).

Synthesis of Polymethacylate-OPS/MMA Copolymers. The bulk radical copolymerization of methyl methacrylate with 0.24 mol % of polymethacylate-OPS was described here as an example: 0.0189 g of $MMA_{6.5}OPS$ and 2 mL of MMA (1.89 g) were charged into a dry glass ampule. After polymethacylate-OPS dissolved completely in the MMA, 0.0142 g of AIBN was added, and the system was flushed with nitrogen and sealed. The solution was heated at 65 °C for 12 h and then 120 °C for another 2 h. In the similar procedures, the copolymers with polymethacylate-OPS contents of 0.47, 0.94, and 1.18 mol % were synthesized, respectively. In addition, the pure PMMA was prepared under the same polymerization conditions for comparison purpose.

Finely ground powder samples of thus synthesized copolymers were successively extracted with acetone using a Soxhlet apparatus for 12 h to remove any possible PMMA homopolymer or unreacted polymethacylate-OPS prior to the structure−property measurements.

For the sake of brevity, in this study, the nanocomposites synthesized with the polymethacylate-OPS content of 0.24, 0.47, 0.94, 1.18 mol % are referred to hereafter as $OPS_{0.24}$-PMMA, $OPS_{0.47}$-PMMA, $OPS_{0.94}$-PMMA and $OPS_{1.18}$-PMMA, respectively.

Cleavage of Si−C Bonds in OPS Macromonomers. The Si−C bonds of polybromo-OPS were cleaved according to the procedure of literature with some modifications:[32] 3.0 g of polybromo-OPS, 2.5 g of KF, 2.4 g of $NaHCO_3$, 25 mL of THF, and 25 mL of methanol were added to a 250 mL round-bottom flask equipped with a magnetic stirring, dry nitrogen inlet and outlet, a condenser, and a dropper. After stirring for 15 min, 20 mL of 30% H_2O_2 was added dropwise over a period of 30 min, and the system was allowed to reflux for another 4 h. The precipitated silica was filtered out, and the solution was concentrated by rotary evaporation to give a liquid brominated-phenol mixture, which composition was analyzed by LC−MS. Similarly, the carboxyl phenyls were cleaved from polycarboxyl-OPS, and were also analyzed by LC−MS method.

Cleavage of Si−C Bonds in PMMA/OPS Nanocomposites. Taking the PMMA/OPS nanocomposite containing 0.24 mol % of OPS as an example: to a 250 mL round-bottom flask equipped with a magnetic stirring, dry nitrogen inlet and outlet, a condenser and a dropper was added 0.5 g of finely ground composite sample, 1.3 g of KF, 1.2 g of $NaHCO_3$, 15 mL of THF, and 10 mL of methanol. After 15 mL of 30% H_2O_2 was added dropwise over a period of 20 min, the system was successively refluxed for 72 h. The solvent was removed to give the white solid, which was extracted with 5 mL of THF three times. The solutions were combined and concentrated, which was slowly poured into a stirred mixed solution of ethanol and deionized water (v/v, 4:1) to precipitate the white polymer. The obtained PMMA was dried under vacuum at 60 °C for 12 h to constant weight (0.4857 g) with a yield about 97%.

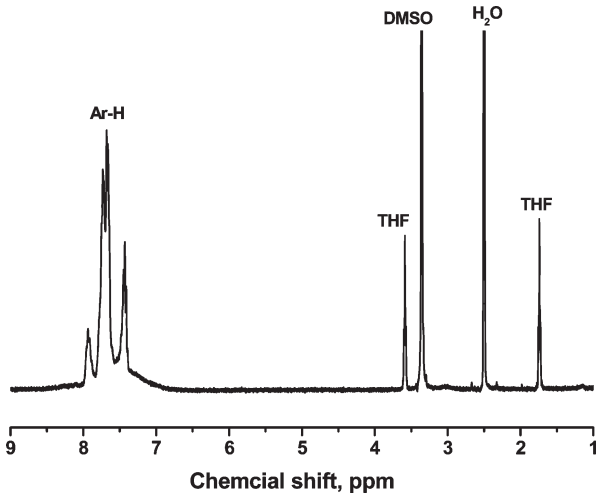

Figure 1. ^1H NMR spectrum of $Br_{8.5}OPS$ with THF as internal standard.

Results and Discussion

Synthesis of Polybromo-OPS. Polybromooctaphenylsilsesquioxane (Br_xOPS), where x is the average number of bromine per OPS molecule, was synthesized from OPS. According to the stoichiometric amount of bromine in the system, the expected x value of Br_xOPS is 9.0 if all the bromines charged are reacted onto the phenyl rings. The real bromine content is measured through ^1H NMR spectrum using tetrahydrofuran (THF) as an internal standard. As shown in Figure 1, the THF protons of $-CH_2-$ and $-O-CH_2-$ appear at 1.73 and 3.59 ppm, respectively, whereas the chemical shift at 7.2−8.1 ppm are attributed to phenyl protons (Ar−H). Accordingly, the average number of hydrogen atom of Ar−H replaced with bromine, i.e., the real x value, can be calculated from the relative peak area of Ar−H and THF−H as well as the amount of THF and Br_xOPS precisely added in the NMR-tube in term to the eq 1:

$$\frac{w(40-x)}{1034+79.9x}\times\frac{72.1}{0.889v\times 4}=\frac{A_{\mathrm{BrOPS}}}{A_{\mathrm{THF}}} \qquad (1)$$

where w and v are the weight of Br_xOPS and volume of THF added, A_{BrOPS} and A_{THF} the integrated peak area of Ar−H and THF−H, respectively, whereas 1034 and 72.1 are molecular weight of OPS and THF, respectively. 79.9, 0.889, and 4 are atomic weight of bromine, density of THF and the proton number in each THF molecule, respectively.

As a result, the x value measured for the polybromo-OPS is 8.5. In order to determine the position of bromine in benzene ring, the Si−phenyl bonds were cleaved from $Br_{8.5}OPS$ by KF/H_2O_2 to produce various phenol compounds, which were collected and afforded for LC−MS analysis. On average, 58% of phenyls are monosubstituted, 24% of phenyls disubstituted, a very small amount of phenyls trisubstituted, and 17% of phenyls unsubsituted (Table 1S, Supporting Information).

Synthesis of Polycarboxyl-OPS ($COOH_yOPS$). Polycarboxyl-OPS was synthesized in two-steps: lithiation of the polybromo-OPS and subsequent carboxylation with carbon dioxide give $COOH_xOPS$ (Scheme 1).

As shown in Figure 2a, the wide peak at 3700−2800 cm^{-1} is attributed to OH stretching of the carboxyl group, whereas the sharp peak at 1699 cm^{-1} is due to the C=O absorption of hydrogen-bonded carboxyl group. A strong absorption at 1587 cm^{-1} is assigned to the benzene ring. In addition, the bands at 1134, 1108, and 491 cm^{-1} belong to the characteristic Si−O−Si vibrations of silsesquioxane cage skeleton.

Scheme 1. Synthesis Route of Polycarboxyl-OPS

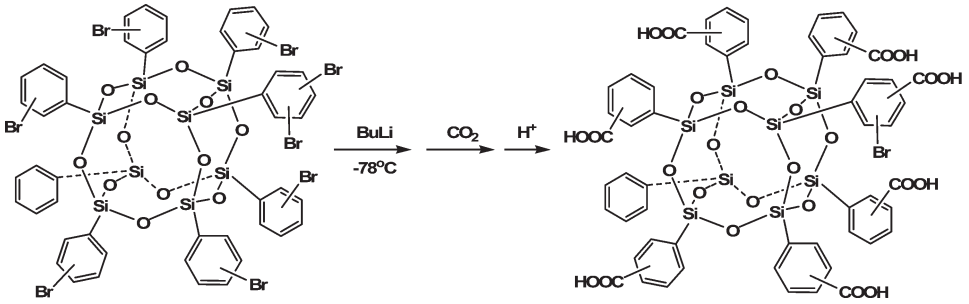

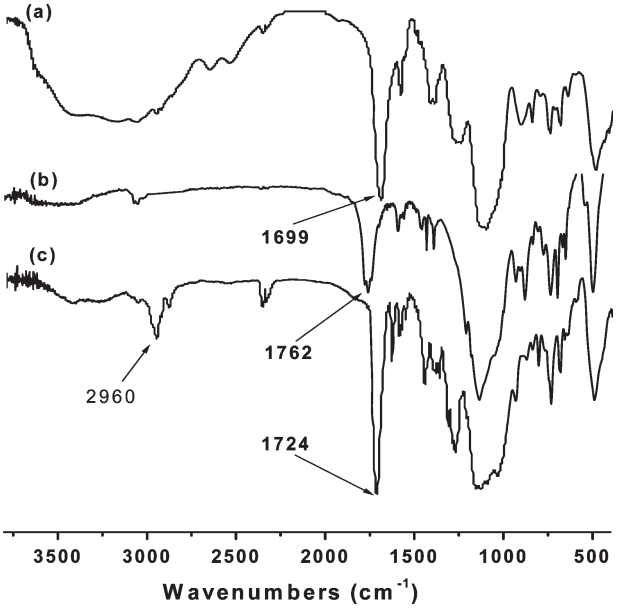

Figure 2. FTIR spectra of (a) $COOH_{6.5}OPS$, (b) $COCl_{6.5}OPS$, and (c) $MMA_{6.5}OPS$.

Similar to polybromo-OPS, $COOH_yOPS$ is also cleaved by KF/H_2O_2, and LC−MS technology is then utilized to analyze the composition of generated organic fragments. The data in Table 2S (Supporting Information) reveal that almost all the monosubstituted phenyls have been converted to carboxyl groups. However, for the di- or tribromo-substituted phenyls, only one bromine atom can be successfully carboxylated. The reason is that, similar to other polybromo-aromatic compounds,[45,46] after one bromine has been reacted with BuLi to form lithium compound, the reactivities of other bromines on the same phenyl are greatly inhibited due to the electropositive effect of lithium-cation so that the further lithiation reaction can not easily take place with BuLi at −78 °C.

NOE-suppressed ^{13}C NMR spectrum of $COOH_yOPS$ is illustrated in Figure 4S (Supporting Information), from which the average number of carboxyl groups in each OPS molecule (y) can be calculated from the integrated areas of corresponding peaks. As is shown, the peaks at 125−150 ppm are assigned to the aromatic carbon atoms, while the characteristic signals of carboxyl C═O are found at 170−180 ppm. Thus, the y value is calculated according to eq 2, and the result is 6.5.

$$y = \frac{48 \times A_1}{A_2} \quad (2)$$

where A_1 and A_2 are the integrated areas of carboxyl carbons and aryl carbons, respectively, and 48 is the whole aryl carbon number included in each OPS molecule.

Synthesis of Polymethacrylate-OPS ($MMA_{6.5}OPS$). The synthesis route of $MMA_{6.5}OPS$ is presented in Scheme 2. At first, the carboxyls in $COOH_{6.5}OPS$ are converted to chlorocarbonyl groups through the reaction with thionyl chloride to yield polychlorocarbonyl-OPS ($COCl_{6.5}OPS$). As shown in Figure 2b, the absorption peak at 1699 cm^{-1} corresponding to C═O stretching vibration of carboxyl group is absent in the spectrum of $COCl_{6.5}OPS$, whereas a new peak at 1762 cm^{-1} attributed to C═O stretching vibration of chlorocarbonyl group appears, indicating that carboxyls of $COOH_{6.5}OPS$ have been smoothly converted to chlorocarbonyl groups. Subsequently, using pyridine as the catalyst, the reaction of polychlorocarbonyl-OPS with 2-hydroxyethylmethacrylate leads to polymethacrylate-OPS macromonomer ($MMA_{6.5}OPS$).

Figure 2c shows the FTIR spectrum of $MMA_{6.5}OPS$. The peaks at 2960 cm^{-1} are assigned to CH_3 and $-CH_2-CH_2-$ stretching vibrations, respectively. A peak at 1637 cm^{-1} is attributed to the C═C stretching of methacrylate group. The appearance of characteristic ester ν C═O at 1724 cm^{-1} and complete disappearance of chlorocarbonyl group at 1762 cm^{-1} suggest the successful synthesis of $MMA_{6.5}OPS$.

$MMA_{6.5}OPS$ is further identified by ^1H NMR method (Figure 3). The peaks at 7.32−7.91 ppm belong to the aromatic protons. The peaks at 3.62 and 4.09 ppm are assigned to the aliphatic $-O-CH_2-CH_2-O-$ protons, the two singlets at 5.65 and 6.05 ppm are attributed to the $C{=}CH_2$ protons, whereas the strong single peak at 1.88 ppm corresponds to the CH_3 of methacrylate group. From the integrated areas of protons from aromatic benzene ring and CH_3 of methacrylate group, on average, the calculated number of methacrylate group in each OPS molecule is 6.36, very close to the expected value of 6.5.

Synthesis and Characterization of OPS/MMA Copolymers. OPS/MMA copolymers were synthesized via bulk free radical polymerization with the $MMA_{6.5}OPS$ content in the nanocomposites of 0.24, 0.47, 0.94, and 1.18 mol %, respectively. The possible PMMA homopolymer and unreacted polymethacrylate-OPS had been removed by extraction with acetone. It is worth noting that after the extracts were concentrated, no any solid can be found, indicating that the formations of three-dimensional networks via cross-linking reactions between $MMA_{6.5}OPS$ and MMA are rapid and effective because of the multiple active methacrylate groups in OPS macromonomer.

Figure 4 shows the FTIR spectra of pure PMMA and OPS/PMMA nanocomposites. In the FTIR spectrum of PMMA, the absorptions at 2996−2850 cm^{-1} are associated to the methyl and methylene groups, while the strong peak at

Scheme 2. Synthesis Routes of $MMA_{6.5}OPS$ and the $MMA_{6.5}OPS$/MMA Copolymer Networks

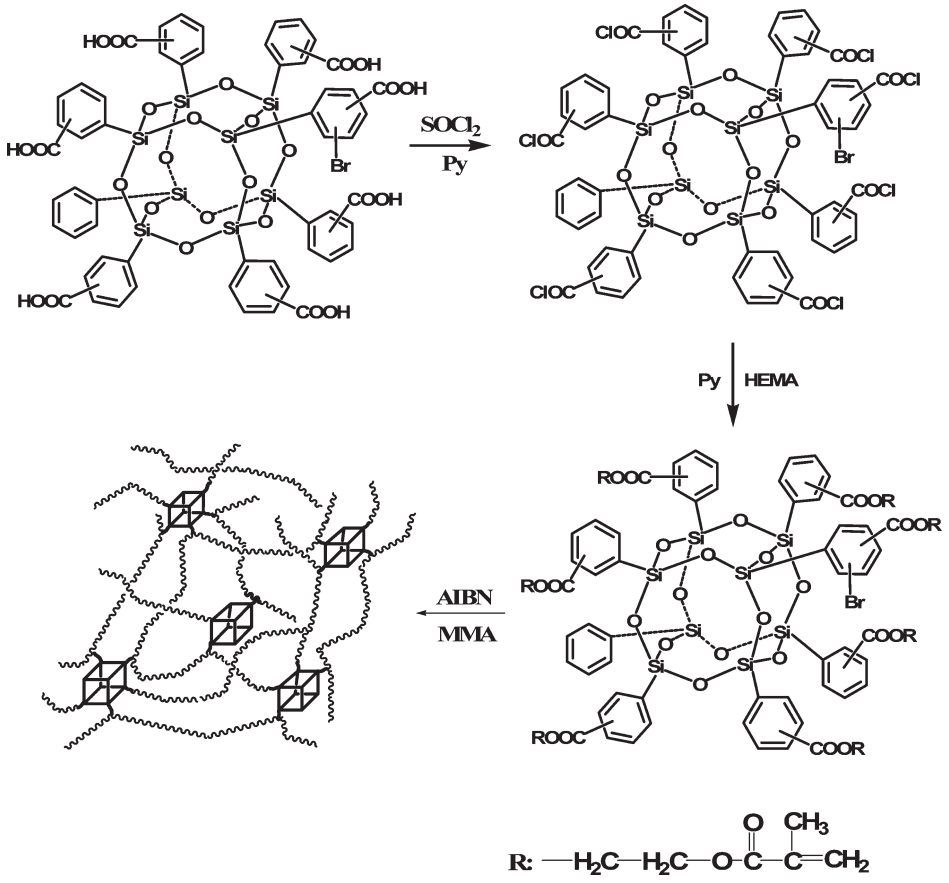

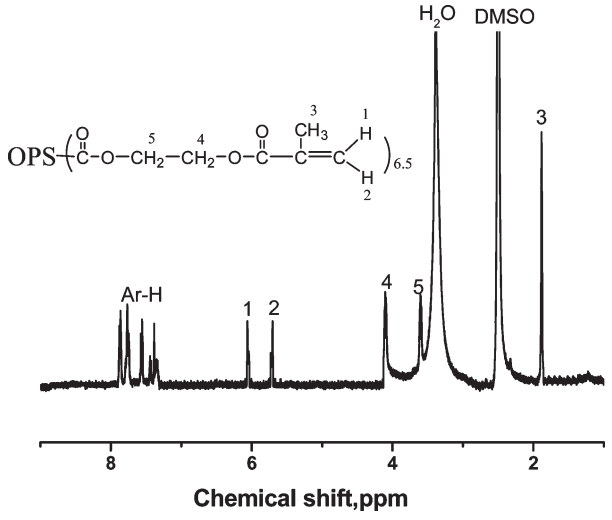

Figure 3. ^1H NMR spectrum of $MMA_{6.5}OPS$.

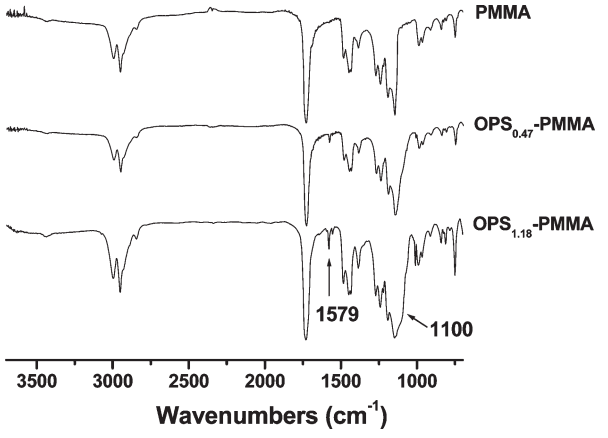

Figure 4. FTIR spectra of pure PMMA and OPS/PMMA nanocomposites.

$1732\ cm^{-1}$ corresponds to the carbonyl stretching vibration of PMMA. As a contrast, in the FTIR spectra of OPS/PMMA nanocomposites, besides the characteristic absorptions of PMMA, the peaks at 1579 and $1554\ cm^{-1}$ can be assigned to the OPS phenyls. Their intensities increase gradually with OPS content. The broadened peak from 1150 to $1100\ cm^{-1}$ is attributed to the characteristic Si−O−Si vibrations of the OPS cage. The above spectra data demonstrate that the OPS moieties are indeed incorporated covalently within PMMA matrix to form a copolymer network.

In this study, the methacrylate group is linked with OPS cage via a flexible $-O-CH_2-CH_2-O-$ spacer. The sufficient freedom offers the dangling methacrylate groups high radical polymerization reactivity. It is observed that the incorporation of only 0.24 mol % $MMA_{6.5}OPS$ gives a cross-linked copolymer that was only slightly swollen on heating in THF and $HCCl_3$, in which $MMA_{6.5}OPS$ and PMMA can dissolve. When the OPS content reaches 0.96 mol %, the product can not swell in the above solvents at all, suggesting that $MMA_{6.5}OPS$ acts as an effective cross-linker to form three-dimensional OPS/PMMA network. This phenomenon is much different from the previous report for polyvinyl-OPS/PMMA copolymer system, in which the

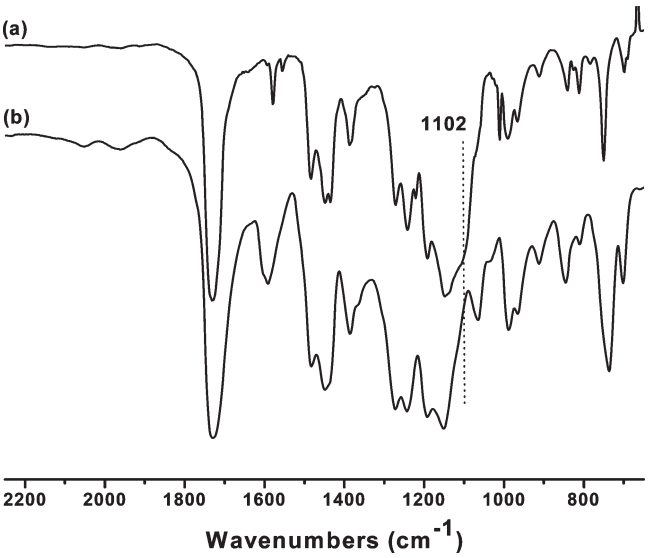

Figure 5. FT-IR spectra of $OPS_{1.18}$-PMMA nanocomposite: (a) untreated; (b) cleaved by KF/H_2O_2.

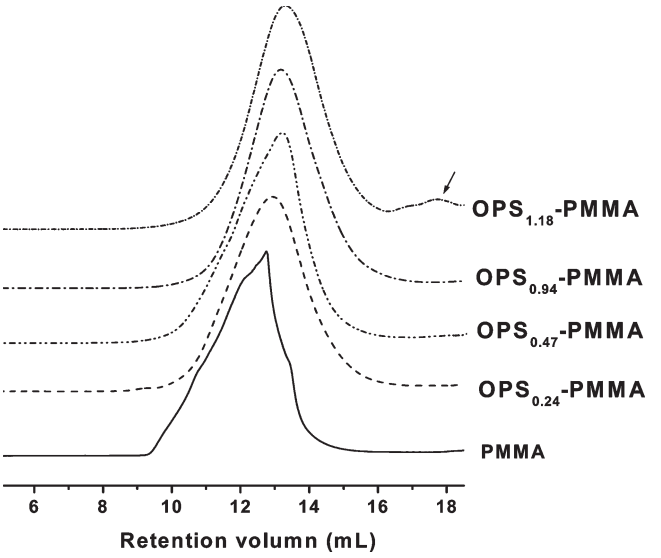

Figure 6. GPC traces of the cleaved products of OPS/PMMA nanocomposites by KF/H_2O_2.

Table 1. GPC Results of OPS/PMMA Nanocomposites Cleaved by KF/H_2O_2

samples	M_n ($\times 10^4$ g/mol)	M_w ($\times 10^4$ g/mol)	M_w/M_n
PMMA	7.52	14.9	1.99
$OPS_{0.24}$-PMMA	4.31	16.1	3.74
$OPS_{0.47}$-PMMA	2.67	7.68	2.88
$OPS_{0.94}$-PMMA	2.43	8.09	3.33
$OPS_{1.18}$-PMMA	2.23	7.89	3.54

vinyl groups are tightly tethered onto the bulky OPS core. Probably, the steric hindrance and restricted motility leads to vinyl group much decreased reactivity so that the polyvinyl-OPS/PMMA only creates branched rather than cross-linked copolymer network even at high contents of octavinyl-POSS over 3 mol %.[21]

In an effort to obtain the structural information about the OPS/PMMA nanocomposites, the finely ground powders were successively treated with KF/H_2O_2 in THF for 72 h to cleave Si−C bonds in OPS core. After removal of insoluble precipitate (SiO_2), the filtrate was poured into a mixed solution of ethanol and water and the white PMMA product is collected. The FTIR spectra demonstrate that the previous Si−O−Si bands at around 1102 cm^{-1} have completely disappeared (Figure 5). In addition, thus obtained PMMA samples were examined by GPC method in order to reveal the growth mechanism of PMMA chains in the $MMA_{6.5}$OPS/MMA polymerization system. As a comparison, the pure PMMA synthesized under the same polymerization conditions has a number average molecular weight (M_n) of 7.52×10^4 g/mol. Apparently, the incorporation of OPS leads to much reduced M_n of PMMA. For example, the M_n value of sample with $MMA_{6.5}$OPS content of 0.94 mol % is only 2.43×10^4 g/mol (Table 1). The high reactivity of attached methacrylate group on OPS makes it be easily initiated by a radical initiator or PMMA chain radical, and the newly generated OPS radical can initiate the polymerization of other MMA monomers. Repeating the above procedure leads to a PMMA cross-linking network. In this way, within this network, a number of OPS moieties can be linked onto one PMMA chain. Because $MMA_{6.5}$OPS is bulky polyfunctional macromonomer, in the initial polymerization stage, the copolymerization of $MMA_{6.5}$OPS with MMA should form branched polymer. The chain entanglement, viscosity increase and bulky OPS volume hinder the propagation ability of the PMMA chains to some extent. As a result, compared to pure PMMA, the PMMA chains in the nanocomposite network exhibit significantly lower molecular weight, and which values are found to continually decrease with the increased OPS content.

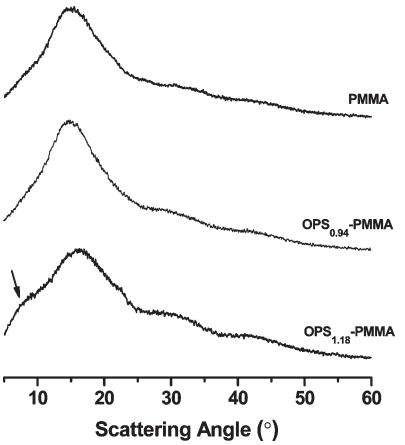

Figure 7. WAXD patterns of pure PMMA, $OPS_{0.94}$-PMMA, and $OPS_{1.18}$-PMMA nanocomposite.

On the other hand, Figure 6 shows that, for the copolymers with low $MMA_{6.5}$OPS contents, the GPC curves present only a single peak, implying that the chain propagation can proceed smoothly to form uniform PMMA network. However, when $MMA_{6.5}$OPS content is over 1.18 mol %, a weak peak corresponding to a short PMMA chain with M_n of 2054 g/mol appears because, in this case, the higher radical concentration in the system makes the viscosity rapidly increase even at the initial polymerization reaction stage, resulting into an increased termination probability of two short PMMA chain radicals.

The WAXD Study of OPS/MMA Nanocomposites. The WAXD diffractograms for PMMA and the PMMA/OPS nanocomposites are illustrated in Figure 7. PMMA obtained through radical polymerization is amorphous and displays a broad peak with 2θ angle at about 14°. The comparison of the diffraction patterns reveals that, for $OPS_{0.94}$-PMMA, its

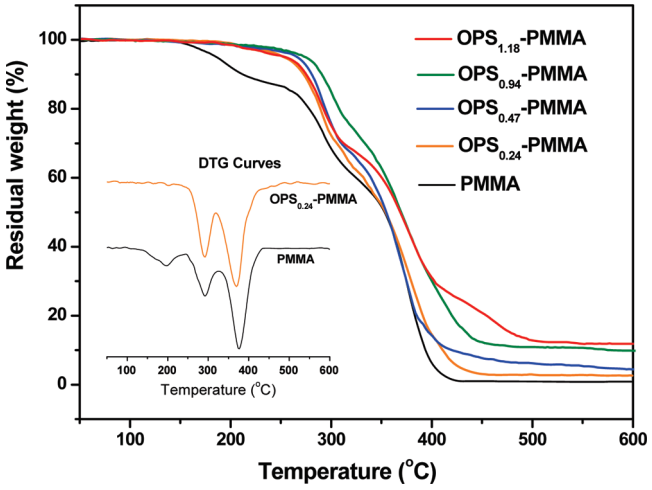

Figure 8. TGA and DTG curves of OPS/PMMA nanocomposites with various OPS content.

Table 2. Thermal Analysis Results of PMMA and OPS/PMMA Nanocomposites

samples	T_g (°C)	$T_{5\%}$ (°C)	$T_{step\text{-}1}$ (°C)	$T_{step\text{-}2}$ (°C)	$T_{step\text{-}3}$ (°C)	RW (wt %)
PMMA	114	183	191	293	367	0.7
$OPS_{0.24}$-PMMA	125	270		296	370	2.0
$OPS_{0.47}$-PMMA	133	271		302	372	4.3
$OPS_{0.94}$-PMMA	135	287		310	372	9.8
$OPS_{1.18}$-PMMA	115	275		304	378	10.3

curve shape is almost the same as that of PMMA, and no any hint of OPS can be observed, implying that OPS moieties are not only covalently cross-linked with PMMA chains but also homogeneously dispersed at the molecular level within the PMMA matrix, which is consistent well with the good transparency of PMMA/OPS nanocomposite samples at low OPS content. However, with the further increase of OPS content, e.g., for $OPS_{1.18}$-PMMA containing 1.18 mol % OPS, it becomes translucent, with some milky and hazy substance throughout the sample. Moreover, a weak peak with 2θ angle at about 8° appears in the curve, which can be assigned to the octaphenylsilsesquioxane core (1−1.1 nm),[47−49] indicating that the aggregation of OPS compound and microphase separation have occurred to some extent.

Thermal Properties of $MMA_{6.5}$OPS/PMMA Nanocomposites. The thermal stabilities of pure PMMA and various PMMA/OPS nanocomposites are compared and studied by TGA under nitrogen at a heating rate of 20 °C/min. Their thermogravimetric and DTG curves are presented in Figure 8 and the data are summarized in Table 2. The pure PMMA exhibits typical three thermal steps of degradation. The first stage at around 191 °C is associated with the cleavage of tertiary ester bond derived from coupling termination. The second one at 293 °C is attributed to the unsaturated vinyl ends caused by the disproportionation termination, and the third one at 367 °C is due to the random scission of main chains, respectively, which behavior is similar to the previously reported results except that the three decomposition steps occur respectively at the increased temperatures since the pure PMMA synthesized in this study has much higher molecular weight than that in the literature.[50,51] Of interest is the observation that, for all the OPS/PMMA nanocomposites, only two thermal decomposition steps appear in the degradation curves. Compared to the pure PMMA, the increase of 5% mass-loss temperature by 87 °C is achieved with only incorporation of 0.24 mol % OPS in the nanocomposite. As a matter of fact, the radical copolymerization of MMA and $MMA_{6.5}$OPS also undergo termination reaction of coupling and disproportionation. However, the high reactivity of polymethacrylate-OPS and its good miscibility with MMA make that the OPS are easily linked with PMMA chain through strong covalent bond and disperse uniformly in the cross-linked network. The low thermal conductivity of OPS because of its inorganic ceramic nature and intrinsic nanoporous structure can hinder the thermal transfer across the sample and effectively retard the degradation of weak bonds which are embedded within the network, leading to the composite materials greatly enhanced thermal stability. Moreover, the samples with high OPS content display obviously increased char yield. However, the increasing trend for the thermal decomposition temperature can not always continue. Relative to $OPS_{0.94}$-PMMA, the $OPS_{1.18}$-PMMA sample exhibits a decreased 5% mass-loss temperature by 12 °C. Just as indicated by the GPC results, relative to the nanocomposites with low OPS content, in the sample of $OPS_{1.18}$-PMMA, there are more number of short PMMA chains and thermally labile groups, such as the tertiary esters derived from coupling termination and the unsaturated vinyl end groups caused by the disproportionation termination, resulting into its decreased thermal stability.

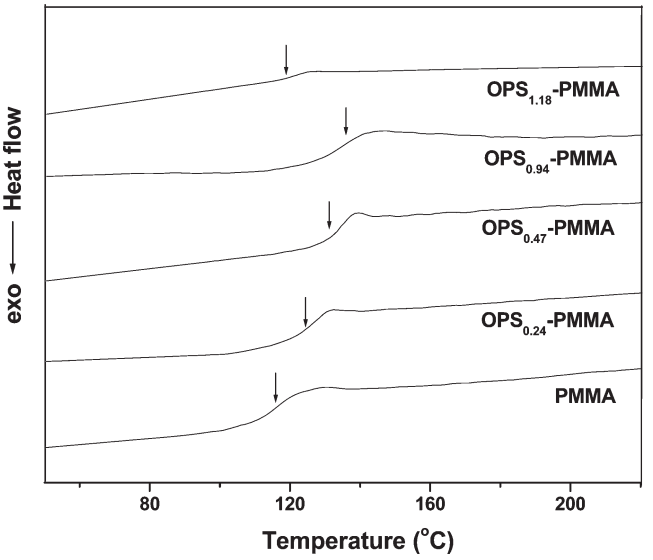

Figure 9. DSC curves of OPS/PMMA nanocomposites with various OPS content.

The previous studies show that the T_g variation of cross-linked PMMA is tightly related to the cross-linker employed. The cross-linking reaction caused by the flexible diol dimethacrylate cross-linker usually can not bring about significant T_g improvement, in some cases, even result in an obvious reduction in T_g. For example, the T_g value of PMMA network derived from the copolymerization between MMA and poly(ethylene glycol) dimethacrylate is only 66.8 °C.[52] On the contrary, the incorporation of rigid bridge between PMMA chains can effectively increase the T_g of PMMA network, depending on the content of cross-linker used in the system.[38,53,54] It was reported that the PMMA film thermally cured via epoxy group had an increased T_g value at 125 °C with 10 mol % cross-linkable component in the network.[53]

The glass transition temperatures (T_g) for the pure PMMA and OPS-modified PMMAs were measured and are presented in Figure 9. As is shown, the T_g values for the modified

PMMAs are obviously shifted from 114 °C of pure PMMA toward higher temperature. Relative to the pure PMMA, the T_g values for composites with OPS content of 0.24, 0.47, and 0.94 mol % increase by 11, 19, and 21 °C, respectively. At lower $MMA_{6.5}OPS$ content, the copolymerizations of $MMA_{6.5}OPS$ and MMA make the reactive methacrylate groups act as multiple claws to anchor PMMA chains onto the rigid OPS core, and thus formed network will restrict the mobility of PMMA segment and significantly increase the glass transition temperatures. For $OPS_{0.47}$-PMMA which incorporates OPS of only 0.47 mol %, its T_g value increases from 114 to 133 °C, exhibiting advantage over the other common cross-linkers reported in the literatures. Nevertheless, the T_g values do not monotonically increase with increased $MMA_{6.5}OPS$ content. It is found that the $OPS_{1.18}$-PMMA sample exhibits an obviously decreased glass transition temperature relative the other three samples. Similar phenomena have also been observed for other POSS/polymer nanocomposite systems, such as POSS−PEG−PMMA,[30] poly(vinyl cinnamate)-POSS,[37] epoxy-POSS,[55] poly(hydroxystyrene-*co*-vinylpyrolidone)-POSS hybrids,[56] which are explained as the increased free volume and chain separation because of bulkiness of POSS group although the real reason still remains a matter of debate.

In our study, the factors, that bulky OPS group opens up the polymer chains and the increased free volume are favorable for the segment motion, can also account for the reduced glass transition temperature of $OPS_{1.18}$-PMMA sample. In addition, the reason arisen from the copolymerization mechanism should be taken into account. The incorporation of high content of polyfunctional OPS cross-linker gives rise to the increased viscosity and rapid gel-formation, leading to the generation of more number of short PMMA chains and a relatively insufficient PMMA cross-linked network. As a result, compared to the OPS/PMMA nanocomposites with lower OPS contents, the glass transition of $OPS_{1.18}$-PMMA sample shifts toward the apparently lower temperature, and the transition range becomes broad.

Conclusions

In this paper, at first, polycarboxyl octaphenylsilsesquioxane with average carboxyl number of 6.5 ($COOH_{6.5}OPS$) was successfully synthesized by two-step reaction: bromination yields polybromo-OPS and subsequent carboxylation leads to the target product. Then, the $COOH_{6.5}OPS$ was further converted to $COCl_{6.5}OPS$ and $MMA_{6.5}OPS$. Their chemical structures were characterized by FTIR, NMR, LC−MS and GPC methods. The polymethacrylate-OPS macromonomers are miscible with methyl methacrylate (MMA), and the mixtures are readily copolymerized to obtain a series of OPS/PMMA copolymers with various OPS content. Thus synthesized nanocomposites are insoluble in any common solvents, demonstrating the formation of cross-linked networks. After being treated in KF/H_2O_2 agent, the PMMA chains were cleaved from the OPS core. For the copolymer systems with low $MMA_{6.5}OPS$ contents, the GPC curves of PMMA chains present only a single peak, implying that the $MMA_{6.5}OPS$ is miscible with MMA, and the chain propagation proceeds smoothly to form uniform PMMA networks, which are well consistent with the WAXD results. The TGA and DSC results reveal that, compared to pure PMMA, after incorporation of very few amount of OPS in PMMA matrix, e.g., 0.94 mol %, the composite exhibits greatly enhanced initial thermal decomposition temperature by 104 °C and apparently increased glass transition temperature by about 21 °C. The study of using polychlorocarbonyl-OPS to form cross-linked polyamides, polycarboxyl-OPS as macromonomer for micro/mesoporous polybenzoxazoles or as curing agent for cross-linked epoxy networks are being undertaken and will be reported subsequently.

Acknowledgment. We thank the National Science Foundation of China (Nos. 50673014 and 20874007) and the Program for New Century Excellent Talents in University of China (No. NCET-06-0280) for financial support of this research.

Supporting Information Available: GPC trace of polybromo-OPS, ^1H NMR spectra of polycarboxyl-OPS, NOE-suppressed ^{13}C NMR spectrum of polycarboxyl-OPS, LC spectra of cleaved products of polybromo-OPS and polycarboxyl-OPS, and their data. This material is available free of charge via the Internet at http://pubs.acs.org.

References and Notes

(1) Tuteja, A.; Choi, W.; Ma, M. L.; Mabry, J. M.; Mazzella, S. A.; Rutledge, G. C.; McKinley, G. H.; Cohen, R. E. *Science* **2007**, *318*, 1615–1622.
(2) Zhang, W. A; Muller, A. H. E. *Macromolecules* **2010**, *43*, 3148–3152.
(3) Escude, N. C.; Chen, E. Y. X. *Chem. Mater.* **2009**, *21*, 5743–5753.
(4) Sulaiman, S.; Bhaskar, A.; Zhang, J.; Guda, R.; Goodson, T., III; Laine, R. M. *Chem. Mater.* **2008**, *20*, 5563–5573.
(5) Cordes, D. B.; Lickiss, P. D.; Rataboul, F. *Chem. Rev.* **2010**, *110*, 2081–2173.
(6) Chen, Q.; Xu, R. W.; Zhang, J.; Yu, D. S. *Macromol. Rapid Commun.* **2005**, *26*, 1878–1882.
(7) Xiao, S.; Nguyen, M.; Gong, X.; Cao, Y.; Wu, H.; Moses, D.; Heeger, A. J. *Adv. Funct . Mater.* **2003**, *13*, 25–29.
(8) Crivello, J. V.; Malik, R. *J. Polym Sci., Part A: Polym. Chem.* **1997**, *35*, 407–425.
(9) Choi, J.; Yee, A. F.; Laine, R. M. *Macromolecules* **2003**, *36*, 5666–5682.
(10) Kickelbick, G. *Prog. Polym. Sci.* **2003**, *28*, 83–114.
(11) Pielichowski, K.; Njuguna, J.; Janowski, B.; Pielichowski, J. *Adv. Polym. Sci.* **2006**, *201*, 225–296.
(12) Phillips, S. H.; Haddad, T. S.; Tomczak, S. J. *Curr. Opin. Solid State Mater. Sci.* **2004**, *8*, 21–29.
(13) Madbouly, S. A.; Otaigbe, J. U. *Prog. Polym. Sci.* **2009**, *34*, 1283–1332.
(14) Brus, J.; Urbanova, M.; Strachota, A. *Macromolecules* **2008**, *41*, 372–386.
(15) Lee, A.; Lichtenhan, J. D. *Macromolecules* **1998**, *31*, 4970–4974.
(16) Mather, P. T.; Jeon, H. G.; Romo, A.; Haddad, T. S.; Lichtenhan, J. D. *Macromolecules* **1999**, *32*, 1194–1203.
(17) Lichtenhan, J. D.; Otonari, Y. A.; Carr, M. J. *Macromolecules* **1995**, *28*, 8435–8437.
(18) Schiavo, S. L.; Mineo, P.; Cardiano, P.; Piraino, P. *Eur. Polym. J.* **2007**, *43*, 4898–4904.
(19) Shockey, E. G.; Bolf, A. G.; Jones, P. F.; Schwab, J. J.; Chaffee, K. P.; Haddad, T. S.; Lichtenhan, J. D. *Appl. Organomet. Chem.* **1999**, *13*, 311–327.
(20) Leu, C. M.; Chang, Y. T.; Wei, K. H. *Macromolecules* **2003**, *36*, 9122–9127.
(21) Xu, H. Y.; Yang, B. H.; Wang, J. F.; Guang, S. Y.; Li, C. *J. Polym Sci., Part A: Polym. Chem.* **2007**, *45*, 5308–5317.
(22) Sellinger, A.; Laine, R. M. *Macromolecules* **1996**, *29*, 2327–2330.
(23) Lichtenhan, J. D.; Otonari, Y. A.; Carr, M. J. *Macromolecules* **1995**, *28*, 8435–8437.
(24) Tsuchida, A.; Bolln, C.; Sernetz, F. G.; Frey, H.; Mulhaupt, R. *Macromolecules* **1997**, *30*, 2818–2824.
(25) Haddad, T. S.; Lichtenhan, J. D. *Macromolecules* **1996**, *29*, 7302–7304.
(26) Lee, A.; Lichtenhan, J. D. *Macromolecules* **1998**, *31*, 4970–4974.
(27) Lee, A.; Lichtenhan, J. D.; Reinerth, W. A. *Polym. Mater. Sci. Eng.* **2000**, *82*, 235–241.
(28) Liu, Y. L.; Lee, H. C. *J. Polym Sci., Part A: Polym. Chem.* **2006**, *44*, 4632–4623.
(29) Baldi, F.; Bignotti, F.; Ricco, L.; Monticelli, O.; Ricco, T. *J. Appl. Polym. Sci.* **2006**, *100*, 3409–3414.
(30) Markovic, E.; Clarke, S.; Matisons, J.; Simon, G. *Macromolecules* **2008**, *41*, 1685–1692.

(31) Zhang, C.; Laine, R. M. *J. Am. Chem. Soc.* **2000**, *122*, 6979–6988.
(32) Brick, C. M.; Tamaki, R.; Kim, S. G.; Asuncion, M. Z.; Roll, M.; Nemoto, T.; Ouchi, Y.; Chujo, Y.; Laine, R. M. *Macromolecules* **2005**, *38*, 4655–4660.
(33) Tamaki, R.; Tanaka, Y.; Asuncion, M. Z.; Choi, J.; Laine, R. M. *J. Am. Chem. Soc.* **2001**, *123*, 12416–12417.
(34) Kim, S. G.; Choi, J.; Tamaki, R.; Laine, R. M. *Polymer* **2005**, *46*, 4514–4524.
(35) Choi, J.; Kim, S. G.; Laine, R. M. *Macromolecules* **2004**, *37*, 99–109.
(36) Won, J.; Tamaki, R.; Kim, S. G.; Laine, R. M. *Chem. Mater.* **2003**, *15*, 3365–3375.
(37) Ni, Y.; Zheng, S. *Chem. Mater.* **2004**, *16*, 5141–5148.
(38) Jantas, R.; Szocik, H.; Stawski, D. *Polym. Bull.* **2005**, *53*, 277–284.
(39) Okaya, O.; Naghash, H. J.; Capaek, I. *Polymer* **1995**, *36*, 2413–2419.
(40) Kelch, S.; Choi, N. Y.; Wang, Z. G.; Lendlein, A. *Adv. Eng. Mater.* **2008**, *10*, 494–502.
(41) Allen, P. E. M.; Bennet, D. J.; Williams, D. R. G. *Eur. Polym. J.* **1992**, *28*, 347–353.
(42) Toepfer, O.; Neumann, D.; Choudhury, N. R.; Whittaker, A.; Matisons, J. *Chem. Mater.* **2005**, *17*, 1027–1035.
(43) Soh, M. S.; Yap, A. U. J.; Sellinger, A. *Eur. Polym. J.* **2007**, *43*, 315–327.
(44) Brown, J. F.; Vogt, L. H.; Prescott, P. I. *J. Am. Chem. Soc.* **1964**, *86*, 1120–1125.
(45) Fournier, J. H.; Wang, X.; Wuest, J. *Can. J. Chem.* **2003**, *81*, 376–379.
(46) Zhang, B. F.; Wang, Z. G. *Chem. Commun.* **2009**, *33*, 5027–5029.
(47) Kopesky, E. T.; Haddad, T. S.; McKinley, G. H.; Cohen, R. E. *Polymer* **2005**, *46*, 4743–4752.
(48) Tamaki, R.; Choi, J.; Laine, R. M. *Chem. Mater.* **2003**, *15*, 793–797.
(49) Choi, J.; Tamaki, R.; Kim, S. G.; Laine, R. M. *Chem. Mater.* **2003**, *15*, 3365–3375.
(50) Kashiwagi, T.; Inaba, A.; Brown, J. E.; Hatada, K.; Kitayama, T.; Masuda, E. *Macromolecules* **1986**, *19*, 2160–2168.
(51) Peterson, J. D.; Vyazovkin, S.; Wight, A. *J. Phys. Chem. B* **1999**, *103*, 8087–8092.
(52) Smith, K. E.; Temenoff, J. S.; Gall, K. *J. Appl. Polym. Sci.* **2009**, *114*, 2711–2722.
(53) Fei, X.; Fu, N.; Wang, Y.; Hu, J.; Cui, Z.; Zhang, D.; Ma, C.; Liu, S.; Yang, B. *Chem. J. Chinese Univ.* **2006**, *27*, 571–574.
(54) Wu, S.; Jorgensen, J. D.; Soucek, M. D. *Polymer* **2000**, *41*, 81–92.
(55) Liu, H. Z.; Zheng, S. X.; Nie, K. M. *Macromolecules* **2005**, *38*, 5088–5097.
(56) Xu, H. Y.; Kuo, S. W.; Lee, J. S.; Chang, F. C. *Polymer* **2002**, *43*, 5117–5124.